University of Arkansas, Fayetteville
ScholarWorks@UARK

Theses and Dissertations

5-2017

Sensitivity of Diffuse Reflectance Spectroscopy to Dose- and Depth-dependent Changes in Tumor Oxygenation after Radiation Therapy

Daria Semeniak
University of Arkansas, Fayetteville

Follow this and additional works at: http://scholarworks.uark.edu/etd

Part of the Biomedical Devices and Instrumentation Commons, and the Radiology Commons

Sensitivity of Diffuse Reflectance Spectroscopy to Dose- and Depth-dependent Changes
in Tumor Oxygenation after Radiation Therapy

A thesis submitted in partial fulfillment
of the requirements for the degree of
Master of Science in Biomedical Engineering

by

Daria Semeniak
Ural Federal University
Bachelor of Engineering in Biomedical Engineering, 2014
Ural Federal University
Master of Engineering in Biomedical Engineering, 2016

May 2017
University of Arkansas

This thesis is approved for recommendation to the Graduate Council.

_____
Dr. Narasimhan Rajaram
Thesis Director

_____   _____
Dr. Kartik Balachandran   Dr. Timothy Muldoon
Committee Member   Committee Member

Abstract

Along with chemotherapy, immunotherapy, and surgery, radiotherapy is one of the most common treatments used against cancer. Around 50% of all cancer patients undergo radiation therapy. While for some patients radiotherapy works efficiently and lead to a complete cancer disappearance, for others treatment outcome may be less favorable due to radioresistance processes happening within a tumor on the molecular level. Radioresistance remains a big challenge for modern oncology. The ability to identify radioresistance at the early stage of radiotherapy would help physicians to improve therapy efficiency. At the current moment, despite the rapid progress in cancer understanding and diagnostic modalities, there is no established technique that would enable early identification of tumor radioresistance.

Tumor oxygenation plays a crucial role for radiotherapy efficiency. We hypothesize that diffuse reflectance spectroscopy (DRS) enabling repeated non-invasive measurements of tumor vascular oxygen saturation can provide surrogate measures of tumor oxygenation to predict tumor response to therapy. The goal of this study is to determine the sensitivity of diffuse reflectance spectroscopy to changes in tumor oxygenation after single-dose radiation therapy in a preclinical tumor xenograft model. We established three specific aims addressing the ability of DRS to provide accurate measures of tumor properties. The first aim is to determine the effect skin thickness on the extraction of optical parameters using one-layer Lookup Table (LUT) model. The second aim is to determine depth- and dose-dependent changes in DRS-measured vascular oxygenation during radiotherapy. The third aim is to determine the association between DRS-measured vascular oxygenation and immunohistochemically assessed intracellular hypoxia.

Our results demonstrate a significant impact of skin thickness on the extraction of optical parameters for short source-detector separations caused by the one-layer assumption of the LUT model. We also detected LUT model failure to identify the absence of melanin when skin is mechanically removed. These findings suggest that existing LUT model needs to be modified to account for the effect of the skin layer. Measurements with different source-detector separations revealed higher concentration of hemoglobin in superficial layer of tumors and blood supply disruption after exposure to 8 Gy of radiation.

Acknowledgements

Table of Contents

I. Introduction

Annually, the American Cancer Society reports more than 500,000 new cases of head and neck cancers (HSNCC) [1]. Early-stage head and neck squamous carcinomas are usually treated by either surgery or x-ray radiotherapy depending on localization and stage of the tumor [2]. Locally advanced head and neck cancers are generally treated with a combination of surgery, chemotherapy, and radiotherapy [3]. Fractioned radiation therapy is a widely-used method of treating head and neck cancers.

In modern oncology, radioresistance remains a big challenge for treating HSNCC. At the current moment, there is no accepted technique that would enable early identification of head and neck tumor radioresistance. A desirable technique should be non-invasive and cost-effective enabling fast repeated examinations. Existing advanced imaging methods to evaluate response to therapy, such as positron emission tomography (PET) imaging of fluorodeoxyglucose (FDG) uptake and magneto-resonance imaging (MRI) are expensive and cannot be used for frequent measurements. Currently, the commonly used method of assessing response to treatment is the anatomical measurement of tumor volume. However, this approach does not shed light on any functional information about processes happening within the tumor during radiotherapy. It is known, that tumor hypoxia significantly affects radiotherapy efficiency and is commonly associated with poor survival of head and neck cancer patients [4–6].Hypoxic tumors are more refractory to radiotherapy than tumors highly saturated with oxygen. Therefore, tumor hypoxia is a potential marker of developing tumor radioresistance. Existing techniques of measuring oxygen level within the tissue are oxygen pO_2 microelectrodes, dynamic contrast-enhanced (DCE)-magnetic resonance imaging (MRI) and blood-oxygen-level dependent (BOLD)-MRI. pO_2 microelectrodes are invasive and cannot be used for repeated examinations. Dynamic contrast-enhanced (DCE)-magnetic resonance imaging (MRI) and blood-oxygen-level dependent (BOLD)-MRI provide indirect measures of deoxygenated hemoglobin. PET imaging [18F]-labeled fluoromisonidazole (FMISO) cannot be repeated frequently and suffers from a low signal to noise ratio [7]. In contrast to listed techniques, diffuse reflectance spectroscopy (DRS) has shown itself capable of repeated non-invasive measurements of tissue vascular oxygenation based on hemoglobin absorption [8,9]. Therefore, DRS is a technique that

potentially can be used for identifying radioresistance of head and neck tumors at the early stage of radiotherapy.

Radiotherapy Principles

Radiotherapy uses different forms of ionizing radiation to kill cancerous cells. Absorption of high-energy particles or waves leads to deposition of energy within the tissue, causing molecular damage. Radiotherapy is usually used in two forms: external beam radiotherapy and internal radiotherapy (brachytherapy). External beam radiation uses high-energy rays of photons (X-ray and gamma) or particles (protons, neutrons, and alpha) that are delivered to the tumor from an outside source such as cathode ray tubes, linear accelerators or cobalt machines. Internal radiotherapy or brachytherapy is delivered from inside the body to the tumor localization by radioactive sources using catheters or seeds. External beam radiotherapy using X-ray is a standard treatment option for the majority of head and neck cancer [12,11].

Radiotherapy kills cancerous cells by two mechanisms called direct and indirect actions. A direct action occurs when macromolecules in a cell such as DNA (deoxyribonucleic acid), RNA (ribonucleic acid), enzymes, or proteins absorb ionizing radiation. As a result of this interaction, macromolecule structures change causing functional abnormalities within a cell. In the presence of oxygen, free radicals in DNA react with the available oxygen to generate a peroxy-radical (DNA–OO•), thus chemically modifying the DNA (oxygen fixation) and causing cell death. In the absence of oxygen, the DNA radical will be reduced, restoring the DNA to its original composition (DNA–H) and leading to cell survival [12]. Thus, the presence of oxygen within cancerous cells is crucial for killing the tumor by direct mechanism. An indirect action happens when high-energy ionizing radiation is absorbed by molecules within a cell. Usually, the molecule initiating indirect action is water molecule (HO_2) that undergoes radiolysis under exposure to radiation. Radiolysis or dissociation of water by radiation forms free radicals, including hydroxyl radicals, which causes DNA damage and damage of other macromolecules important for cell survival.

Radiation damages both normal cells and cancer cells. The goal of radiotherapy is to maximize the effect of radiation on cancer cells and minimize the effect of radiation on normal cells. In normal cells, DNA reparation processes are usually more efficient than in abnormal cells. Therefore, radiation is more deleterious for tumor cells rather than healthy tissue.

Fractioned Radiation Therapy Principles

Radiotherapy is usually performed in a fractioned regime where radiation dose is split into several smaller doses. Typically, radiation therapy fractioned regime incorporates daily fractions of 1.5 to 3 Gy given for the period of 4-5 weeks. The idea behind fractioned regime is to improve treatment outcome by reoxygenating and hence radiosensitizing previously hypoxic cancer cells. The mechanism of reoxygenation has been attributed to various reasons, such as destruction of oxygenated tumor cells, decreased overall oxygen consumption, and increased tumor perfusion. As a result of reoxygenation, more oxygen in blood vessels is available for survived cancer cells making them more sensitive to radiation with the next exposure. In several studies, it has been shown that tumor oxygenation has a substantial impact on the survival rate of cancer patients treated with radiotherapy [4,13,14]. Therefore, tumor reoxygenation between radiation fractions is critically associated with treatment response [4,6,15–18]. Developing technologies to quantify tumor reoxygenation could significantly improve clinician's ability to identify patients having poor response to radiation therapy on the early stage of the treatment.

Existing Techniques for Measuring Tissue Oxygenation

Hypoxia is an important cause of radiation treatment failure in head and neck cancer [4,13,14]. Information about the level of hypoxia in tumor would give an important insight for oncologist regarding tumor sensitivity to radiation. However, existing technologies for measuring tissue oxygenation have certain limitations that make them impossible to use in patient care.

The oxygen-sensing pO_2 microelectrodes are invasively implanted into the tissue to measure oxygen concentration based on polarography. It is an accepted and reliable tool for understanding oxygen metabolism in different tissues and organs. pO_2 microelectrodes have helped to establish a wealth of

knowledge of hypoxia and its role in poor disease-free survival in HSNCC [4,19–21]. Although pO_2 microelectrodes enable absolute measures of oxygenation, they are invasive and provide assessment of hypoxia for a limited area of the tissue. Therefore, pO_2 electrodes are not suitable for repeated clinical measurements.

Two advanced imaging techniques enabling non-invasive measures of oxygenation such as dynamic contrast-enhanced (DCE)-magnetic resonance imaging (MRI) and blood-oxygen-level dependent (BOLD)-MRI have also been shown to be able to provide information about tumor hypoxia [22–24]. DCE-MRI is based on registering the intensity of contrast agent accumulated in tissue microvasculature, thereby providing indirect measures of tissue oxygenation [22]. It was previously demonstrated that DCE-MRI could be used for prediction of response to radiotherapy in head and neck cancer [25]. In (BOLD)-MRI, the source of contrast is deoxyhemoglobin [23]. Deoxygenated hemoglobin increases the MRI transverse relaxation rate of water in blood and surrounding tissues. (BOLD)-MRI provides the assessment of hypoxia based on the assumption that deoxygenated hemoglobin concentration is proportional to pO_2. The main drawback of both MRI modalities, DCE- and (BOLD)-MRI, is that they provide indirect measures of tissue oxygen status.

Tumor hypoxia imaging can be also accomplished by positron emission tomography (PET) using [18F]-labeled fluoromisonidazole (FMISO). FMISO binds to macromolecules within cells where pO_2 is less than 10 mm Hg. However, the technique cannot be repeated frequently because of the accumulation of contrast agent in normal tissue. This method also lacks sufficient signal to noise ratio [7].

In comparison to DCE-MRI, (BOLD)-MRI, and PET imaging, diffuse reflectance spectroscopy has several substantial advantages. DRS is a cost-effective, compact system enabling non-invasive fast repeated measurements of both oxygenated and deoxygenated hemoglobin concentrations in tumor vasculature, thereby providing measures of tissue vascular oxygenation.

Diffuse Reflectance Spectroscopy (DRS) Principles

Diffuse reflectance spectroscopy (DRS) is widely used for noninvasive characterization of tissue optical properties. DRS is an optical fiber-based technique that enables repeated measurements of tissue

4

oxygenation based on optical absorption and scattering properties. DRS reflectance spectrum is used to determine tissue reduced scattering coefficient, tissue concentrations of hemoglobin (total hemoglobin, cHb, deoxygenated hemoglobin, dHb, and oxygenation hemoglobin, HbO_2), and tissue oxygen saturation (sO_2).

In DRS, light of the visible range is generated by light source (e.g. halogen lamp) and sent to the tissue through the optical fiber probe. Typical fiber probe for DRS contains source fibers conducting light from the light source to the tissue and fibers collecting light reflected back from the tissue. Within tissue, light undergoes multiple light-tissue interactions including scattering and absorption. Within the visible range, there are two main contributors to the absorption of light by tissue: hemoglobin and melanin. Melanin is the main absorber of light in epidermis of the tissue whereas hemoglobin is exclusively located in blood vessels and contributes to the absorption of light by dermis. Blood in vessels comprises two types of hemoglobin: hemoglobin bound to oxygen or oxygenated hemoglobin HbO_2 and unbound hemoglobin called deoxygenated hemoglobin dHb. These types of hemoglobin have different absorption spectra that can be easily distinguished in the wavelength range of 500-600 nm (Fig. 1). In this wavelength range, deoxygenated hemoglobin has only single peak at 580 nm when oxygenated hemoglobin has two peaks at wavelengths 550 and 600 nm. Differences in the spectral shape of dHb and HbO_2 enables optical measurements of blood vessel oxygen saturation SO_2 calculated as a ratio between concentration of oxygenated hemoglobin and concentration of total hemoglobin:

$$SO_2 = 100\% \times \frac{HbO_2}{dHb + HbO_2}, \qquad (1)$$

As well as absorption, scattering greatly contributes to the reflectance. The main sources of scattering within the tissue are filamentous proteins: keratin in epidermis and collagen in dermis. Among other tissue components that cause scattering of light are melanosomes in epidermis, cell nuclei, cell walls, mitochondria, etc. [26].

In optics, scattering in tissues is usually described by reduced scattering coefficient:

$$\mu'_s(\lambda) = \mu'_s(\lambda_0) \times (\frac{\lambda}{\lambda_0})^{-B}, \qquad (2)$$

where μ'_s is the reduced scattering coefficient at wavelength λ and B is scattering power related to scattering particle size.

Absorption in tissues is usually described by absorption coefficient and calculated using the following equation:

$$\mu_a(\lambda) = [cHb] \times [\varepsilon_{HbO_2}(\lambda) \times [SO_2] + \varepsilon_{Hb}(\lambda) \times (1 - [SO_2]), \qquad (3)$$

Where $\mu_a(\lambda)$ is absorption coefficient at wavelength λ, cHb is the total hemoglobin concentration, ε_{HbO_2} and ε_{Hb} are the extinction coefficients of oxy-hemoglobin HbO_2 and deoxy-hemoglobin dHb, respectively, and sO_2 is oxygen saturation.

DRS enables measurements of reflectance which characterizes light which underwent multiple light-tissue interactions. Reflectance is calculated as a ratio between the intensity of the reflected light and intensity of light sent to the tissue.

The sampling depth of diffuse reflectance spectroscopy depends on source-detector separation of the optical fiber probe and the optical properties (absorption and scattering) of the interrogated tissue. Typically tissue optical absorption and scattering decrease with higher wavelength of light. Therefore, light travelers deeper into the tissue in the near-infrared diapason (NIR). DRS for cancer applications uses light of the visible spectral range what enables measures of tissue parameters on the depths of millimeters [27].

Existing DRS Studies of Tumor Oxygenation during Radiotherapy

In the past, several studies have demonstrated that DRS has a potential to register changes in tumor oxygenation during radiotherapy and, therefore, can be used for predicting radiotherapy outcome [8,9,27]. Vishwanath et al have shown that DRS is able to register differences in oxygenation between tumors completely responding to radiation and tumors having a partial response [9]. In particular, complete

responders have been demonstrated to have a higher increase in oxygenation in comparison to controls and partial responders during 7 days posttreatment. Hu's used DRS to test whether oxygen kinetics can be correlated with radiotherapy outcome and found that locally controlled tumors have significantly faster oxygenation after the treatment [27]. However, in this study, the total dose for fractioned therapy was chosen based on the tumor control dose 50% (TCD50) and then split into 5 doses from 7.5 to 13.5 Gy per fraction. The chosen doses do not reflect the real clinical situation where patients having head and neck cancers typically receive dose per fraction from 1.5 to 3 Gy (for 4-5 weeks). Therefore, there is a need to determine DRS sensitivity to changes in tumor oxygen saturation using clinical doses to replicate clinical conditions.   In our study, we conducted single-dose radiotherapy of two different doses D = 2 Gy and D = 8 Gy to determine the sensitivity of DRS to conventional doses of radiation used in clinic.

Lookup Table LUT–based Inverse Model for Extracting Optical Parameters

Spectral analysis of DRS measurements requires an inverse model to extract tissue optical properties from the obtained reflectance. One of the most commonly used methods is Monte Carlo simulation of photon transport within the tissue [28]. However, in our studies we use lookup table LUT–based inverse model which has shown to have excellent agreement between the expected and extracted values of the optical parameters for a variety of different source-detector separations [29]. The detailed description of LUT generation is described elsewhere [29]. Briefly, LUT is created by measuring reflectance values of tissue phantoms with known optical characteristics: reduced scattering coefficient μ_s' and absorption coefficient μ_a. As a result, generated lookup table contains values of reflectance and its corresponding scattering and absorbing coefficients. When reflectance of real tissue is measured, this table is used to find tissue μ_s' and μ_a.

Impact of One-layer Assumption on Diffuse Reflectance Spectroscopy

LUT model is a one-layer model and it is based on the assumption that tissue is homogeneous medium containing absorbing and scattering components. However, in real situation tumors are two-layer objects consisting of epidermal layer and dermis. In real tissues, melanin is located in the top layer of the tissue whereas hemoglobin is only located in blood vessels. When one-layer LUT is applied to two-layer

objects, it is important to study errors caused be one-layer assumption. In our study, we are addressing the applicability of one-layer model for measuring optical parameters of two-layer objects.

Thesis Statement

It was previously shown that DRS has a potential to register changes in tumor oxygenation during radiotherapy and able to differentiate between tumors responding and not responding to radiation based on vascular oxygenation measurements [9,27]. Therefore, we hypothesize that optical measurements of vascular oxygenation measured by DRS can provide crucial information regarding tumor response to treatment at the early stage of radiotherapy. The overall goal of our laboratory is to develop a multi-depth diffuse optical spectroscopy (MDDRS) to determine biomarkers of radiation resistance in head and neck tumors. However, on the way to achieving this long-term goal, it is important to determine the sensitivity of DRS to changes in tumor oxygenation during radiotherapy.

Sensitivity and accuracy of DRS mostly depends on the chosen source-detector separation of the optical fiber probe and the selected model for extracting optical parameters from obtained reflectance spectra. LUT model used for extracting optical parameters from DRS-measured reflectance spectra is based on one-layer assumption and, therefore, requires close consideration of possible errors associated with the simplification of tissue structure. Along with tissue properties, source-detector separation greatly affects the sampling depth of DRS spectroscopy.

Therefore, the goal of this project is to study the sensitivity of DRS spectroscopy to changes of vascular oxygenation after radiotherapy. To achieve these goal, we established three specific aims addressing important aspects of DRS sensitivity:

1. To determine the effect skin on extraction of optical parameters using one-layer LUT model;
2. To determine depth- and dose-dependent changes in vascular oxygenation during radiotherapy using DRS;
3. To determine the association between DRS-measured vascular oxygenation and immunohistochemically assessed intracellular hypoxia.

II.   Materials and Methods

Animal Study Protocols and Optical Measurement Schedule

To determine the effect of skin on DRS-measured optical properties, 5 Balb/c mice were injected in the flank with a subcutaneous bolus of 4T1 murine breast cancer cells (1×10^6 cells suspended in 100 µl of serum- and media-free saline) and another 5 Balb/c mice were injected in the flank with a subcutaneous bolus of 67NR murine breast cancer cells (2×10^6 cells suspended in 100 µl of serum- and media-free saline). DRS spectroscopy using 350 µm SD probe was conducted during tumor growth every day until tumors reached 200 mm^3 in volume. Once tumor volumes reached 200 mm^3, skin layer of 6 mm in diameter was removed from the same spot where DRS spectroscopy was previously measured. After skin excision, DRS was performed on the same area to obtain measurements of optical parameters without skin. After that, mice were euthanized using carbon dioxide (CO_2) gas.

Additional study was conducted to determine the effect of source-detector separation on DRS measurements with and without the skin. In this study, 10 Balb/c mice were injected in the flank with a subcutaneous bolus of 67NR murine breast cancer cells (750,000 cells suspended in 100 µl of serum- and media-free saline). Once 5 mice reached tumor volume of 200 mm^3, DRS measurements using 2.25 mm SD probe were conducted to measure tumor optical characteristic with and without skin layer. Once another 5 mice reached the volume of 600 mm^3, they underwent the same procedure where they underwent DRS spectroscopy with and without epidermis on the top of tumors.

To determine depth- and dose-dependent changes in tumor oxygenation 30 Balb/c mice were injected with a subcutaneous bolus of 4T1 murine breast cancer cells (750,000 cells suspended in 100 µl of serum- and media-free saline). Once tumor volume reached 100 mm^3, five mice were selected for tumor excision and following hypoxia immunostaining. When the rest of mice reached 200 mm^3 tumor volume, five mice were selected as a control group for tumor excision and hypoxia immunostaining, and the remaining 20 mice were equally separated into groups that underwent 2 and 8 Gy single-dose radiation therapy with the following tumor excision and immunostaining. DRS optical measurements using 1.5 mm

and 2.25 mm source-detector separations were conducted for each group at tumor volumes of V = 100 mm^3 and V = 200 mm^3 as well as right before tumor excision.

All experiments were conducted in accordance with protocols (#15035) approved by the Institutional Animal Care and Use Committee.

Diffuse Reflectance Spectroscopy System

The system used for measuring the diffuse reflectance (Fig. 2C) consisted of flame VIS-NIR fiber optic spectrometer (Ocean Optics), tungsten halogen light source for the VIS-NIR (Ocean Optics), and fiber-optic probe with source-detector separations of 350 µm (Fig. 2A), 1.5 mm, and 2.25 mm (Fig. 2B). 20%, 80%, and 80% reflectance standards were used to correct the wavelength-dependent daily changes in lamp throughput and calculate diffuse reflectance for SD = 350 µm, SD = 1.5 mm, and SD = 2.25 mm, respectively

Tissue Phantom Model

Optical properties extraction was performed using a lookup table (LUT)–based inverse model [29]. To generate LUT models for SD separations of 350 µm, 1.5 mm, and 2.25 mm liquid homogeneous calibration and validation phantoms were created and measured using DRS. Calibration phantoms consisted of 5 solutions with varying concentrations of the absorber (mix of blue, red and yellow food dyes) and scatterer (1 µm diameter polystyrene spheres, 07310-15, Polysciences, Inc., Warrington, Pennsylvania). Validation phantoms consisted of 5 solutions with varying concentrations of hemoglobin as an absorber and polystyrene spheres as a scatterer. Hemoglobin used for creating validation phantoms is water soluble ferrous hemoglobin powder (H0267, Sigma, MO). As a result, generated LUT tables contain all measured reflectance values and its corresponding combination of scattering and absorbing coefficients. Obtained tables were used for fitting optical spectra obtained from animals.

Radiotherapy System

Radiotherapy was performed using a biological X-ray radiator (X-RAD 320, Precision X-ray). Mice were anesthetized using a mixture of isoflurane and room air (1.5% v/v) introduced into the radiation an access port. All parts of the animal except the tumor were shielded using lead blocks (Fig. 3). Up to 4 mice can be irradiated at a time. The radiation beam has minimal variations within the 20x20 cm illumination field. Exposure time for a 2 Gy dose is approximately 2 minutes.

Immunohistochemical Measurement of Intracellular Hypoxia

For hypoxia staining, mice were injected intraperitoneally with pimonidazole (at a dose of 60 mg/kg, solution of 12 mg/ml), a hypoxia marker binding thiol-containing proteins in hypoxic cells with pO_2 < 10 mm Hg (Hypoxyprobe-Red549 Kit (Dylight™549-Mab), NPI, Inc, Burlington, MA). About 1 hour after injection, mice were euthanized and the tumors were resected, embedded in OCT compound, and snap-frozen by placing into a container with isopentane immersed in liquid nitrogen and cooled down to the temperature of -80 C°. Then, tumors were stored for future histology and immunohistochemistry at -80 C°. Based on the sampling depth of SD separations of 1.5 mm and 2.25 mm, tumor slices were obtained from depths of d=0.8 mm and d=1.8 mm, respectively. From each depth, first slice was extracted for H&E staining (hematoxylin & eosin) (Fig. 4A) to determine necrotic fraction and second slice was extracted for antibody staining of pimonidazole (Figure 4, B) to determine hypoxic fraction. This is done to ensure that we are comparing optical measurements to the hypoxic fraction at the corresponding sampling depth of the probe. Hypoxic fraction within a slice is quantified as the ratio of pimo-bound area to total area:

$$HF = \frac{Hypoxic\ tumor\ area}{Total\ tumor\ area - Necrotic\ tumor\ area} \times 100\%, \qquad (4)$$

Where hypoxia area was quantified based on number of fluorescent pixels in pimonidazole images (Fig. 4D), total area was calculated as total number of pixels from images of H&E staining (Fig. 4C), and necrotic area was calculated as total number of pixels within necrotic areas of H&E staining.

Snap-frozen tumors were sliced into sections of 10 µm using a cryotome (CM1850; Leica, Inc., Nussloch, Germany). Tumor was oriented in such a way that slicing starts from the skin side to ensure slice extraction from the depths of d=0.8 mm and d=1.8 mm corresponding to sampling depths of SD = 1.5 mm and SD = 2.25 mm.

Statistical Methods

Multi-factor ANOVAs was used to compare the vascular oxygenation and total hemoglobin concentration across cell lines, SD configurations, and different doses of radiation. Post-hoc Tukey HSD tests was used to evaluate significant differences in optical properties between the tumor groups. The associations between optically measured hemoglobin concentration, scattering power, melanin concentration and immunohistochemically quantified hypoxic fraction were determined using Pearson correlation coefficient (R). Statistical significance was tested based on a null hypothesis that $R = 0$ for uncorrelated data.

Nonparametric Mann–Whitney–Wilcoxon test was used to compare quantified hypoxic fractions at different tumor volumes and after exposure to radiation.

For all types of statistical analysis, the level of significance is $p < 0.05$.

III.   Results

The Effect of Mouse Skin on Extraction of Optical Parameters Using DRS with SD = 350 µm

The first aim was to determine the effect of skin on extraction of optical parameters using one-layer LUT model. One-layer LUT model was applied to fit two-layer (tumors with skin) and one-layer (tumors with skin removed) spectra obtained from animals.

Fig. 5 demonstrates representative diffuse reflectance spectra measured from an individual tumor before and after skin was removed using source-detector separation SD = 350 µm. We observed decrease in the magnitude of reflectance caused by skin resection. Mouse skin contains multiple sources of light scattering in visible range: filamentous proteins such as keratin and collagen, melanosomes, cell nuclei, cell walls, mitochondria, and other scattering structures. The observed drop in reflectance magnitude can be associated with decreased scattering due to the removal of these scattering components.

We applied one-layer LUT model to fit one- and two-layer tumor spectra measured by DRS using SD = 350 µm and extracted tumor characteristics such as scattering, scattering power, melanin concentration, hemoglobin concentration cHb, and oxygen saturation sO_2. Fig. 6 shows mean values of the extracted parameters before and after the skin was removed from tumors. From the obtained data, we observed nonsignificant changes in scattering power, melanin concentration, and oxygen saturation and significant changes in scattering and hemoglobin concentration after skin removal. First, we observed a significant decrease (p-value < 0.05) in scattering that is consistent with the change in spectral shape for individual tumors (Fig. 6A). Second, we observed an unexpected nonsignificant increase in measured melanin after the skin was resected (Fig. 6C). Melanin is mainly located in the epidermis and it was not expected to detect melanin contribution to the DRS-measured parameters of one-layer tumors. The observed increase in melanin concentration indicates LUT-model failure to sense the absence of melanin. Third, we also observed a significant increase in measured hemoglobin concentration (p-value < 0.01). This indicates a higher sensitivity of DRS to cHb if there is no skin on the top of a tumor (Fig. 6D).

To determine whether one-layer assumption would cause errors in the extraction of optical parameters we studied the correlations between extracted hemoglobin concentration, scattering power, and melanin when one-layer LUT is applied to fit two-layer animal spectra. We hypothesized that cHb, scattering power, and melanin concentration are not physiologically related parameters and the cross-talks between them may indicate model errors caused by one-layer assumption. The correlation between B as a scattering characteristic and melanin concentration as an absorption characteristics is especially important for the consideration due to the similarity in the spectral shapes of these two parameters. Due to similar power law spectra of scattering coefficient and melanin absorption, LUT model is often incapable of distinguishing between scattering and absorbing contributions to the reflectance leading to underestimation of some parameters and overestimation of others. To study correlations between cHb, scattering power, and melanin concentration we plotted measured pairs of cHb, B, and melanin concentration and calculated corresponding Pearson correlation coefficients (Fig. 7A, 7B). In Fig. 7A cHb and melanin have Pearson coefficient $R = 0.7269$ (p-value = 0.0265). In Fig 7B, scattering power B and melanin concentration have Pearson correlation $R = 0.844$ (p-value = 0.0042). We noticed that the correlation between cHb and melanin is caused by an outlier point when values of cHb and melanin concentrations are high. The contribution from the outlier data point makes it difficult to unequivocally conclude the relationship between extracted hemoglobin and melanin concentrations. In Fig. 7B we see the clear correlation between scattering power and melanin concentration. As was stated before, the correlation between B and melanin is unexpected and unwanted result indicating an error caused by one-layer assumption.

To make sure that correlation between B and melanin is caused by the one-layer assumption we applied one-layer LUT model to extract one-layer properties when skin was removed from tumors (Fig. 7C, 7D). As the result, we did not observe any significant correlation between cHb and melanin (Fig. 7C), nor did we observed the correlation between B and melanin (Fig. 7D). We concluded that for SD = 350 μm applying a one-layer model to fit one-layer spectra does not produce errors associated with the one-layer assumption.

14

The Effect of Source-detector Separation on Extracted Optical Parameters

To test the effect of source-detector separation on the extracted optical parameters another experiment was conducted where we used the probe with longer source-detector separation SD = 2.25 mm (approximate sampling depth is d = 1.8 mm). Data obtained for SD = 2.25 mm was compared with results obtained for SD = 350 μm that were described above.

In Fig. 8, representative spectra from two individual animals are shown. Fig. 8A demonstrates DRS spectra from an animal having tumor volume V = 200 mm^3 before and after the skin was removed from the top of the tumor. Fig. 8B demonstrates DRS spectra for an animal having tumor volume V = 600 mm^3 before and after the skin was resected from the top of the tumor. For both individual measurements from groups of mice having different tumor volumes, we observed a decrease in reflectance magnitude caused by epidermis elimination. This observation is consistent with the result obtained for SD = 350 μm. The overall drop of the reflectance magnitude indicates decreased scattering in tumors that were devoid of the epidermal layer. We also found that compared to diffuse reflectance measured by the probe with SD = 2.25 mm, the drop in the reflectance magnitude caused by skin removal for SD = 350 μm is greater (Fig. 9). This observation may be indicative of the higher sensitivity of SD = 350 μm to the skin layer caused by superficial sampling depth of this probe that is approximately d = 116-175 μm. It was shown that Balb/c female mouse skin thickness is equal to 520±30 μm [30]. In our experiments, mouse skin stretched on the top of a tumor varies from 100–300 μm. Therefore, it was expected that skin layer could greatly contribute to the DRS measurements obtained by short source-detector separations SD = 350 μm.

Fig. 10 shows extracted optical parameters from DRS-measured reflectance using probe with SD = 2.25 mm. We observed nonsignificant changes in scattering, scattering power, melanin concentration, and oxygen saturation and significant change in extracted hemoglobin concentration after the skin was removed. First, we observed a slightly greater decrease in scattering in the group measured at the volume V = 200 mm^3 compared to the group measured at the volume V = 600 mm^3 (Fig. 10A). We suggest it may be associated with the skin thickness variations. During tumor growth skin on the top of a tumor becomes stretched and the skin thickness becomes thinner. Therefore, for tumors at the volume V

= 600 mm^3 thinner skin contributes to the DRS-measured reflectance with the less extent compared to the group with V = 200 mm^3. Second, in Fig. 10C, we also observed lower melanin concentration for the group measured at the V = 600 mm^3 which indicates thinner skin layer at higher tumor volume. Third, it is important to note that similarly to the SD = 350 μm, for SD = 2.25 mm we observed deceptive melanin contribution to one-layer tumor spectra even when the skin was removed (Fig. 10C). This observation confirms LUT-model failure to identify the absence of melanin. Similarly to SD = 350 μm, skin removal caused higher sensitivity to cHb for SD = 2.25 mm (p-value < 0.05 for V = 200 mm^3, p-value < 0.01 for V = 600 mm^3) (Fig. 10D). In Fig. 10E, we found nonsignificantly lower measures of sO$_2$ for tumor volume V = 600 mm^3 which is indicative of increased consumption of oxygen caused by tumor growth.

In Fig. 11, we compared data obtained for 67NR mice at the volume V = 200 mm^3 using 350 μm and 2.25 mm source-detector separations before and after the skin was removed. We observed higher measures of scattering for SD = 350 μm compared to SD = 2.25 mm (p-value < 0.001 for measures with skin, p-value < 0.01 for measures without skin) and a greater decrease in scattering for SD = 350 μm after the skin was eliminated (p-value < 0.01) (Fig. 11A). These two observations indicate higher sensitivity of SD = 350 μm to the presence of the skin layer which we associate with its superficial sampling depth. We observed similar measures of hemoglobin concentrations for SD = 350 μm and SD=2.25 mm (Fig. 11D). Data obtained for SD = 2.25 mm shows higher sO$_2$ compared to SD = 350 μm which may be caused by physiological differences on different depths of tumors (p-value < 0.05 for measures with skin, p-value < 0.05 for measures without skin) (Fig. 11E).

To test errors caused by one-layer assumption for SD = 2.25 mm, we plotted measured pairs of cHb, scattering power, and melanin concentration when one-layer LUT was applied to fit two-layer tumor spectra (Fig. 12). As a result, we did not observe any significant correlations between these properties when one-layer model is applied to fit two-layer spectra (Fig. 12A, 12B). We also did not observe any correlation between cHb, B, and melanin when the one-layer model was used to fit one-layer spectra of tumors lacking skin (Fig. 12B). These results obtained for SD = 2.25 mm in conjunction with the findings for SD = 350 μm indicate that the effect of one-layer assumption is greater for smaller source-detector separations having superficial sampling depths. In other words, for small source-detector separations, the

16

one-layer assumption is a source of errors leading to underestimation or overestimation of extracted two-layer properties.

Depth- and Dose-dependent Changes in Vascular Oxygenation during Radiotherapy Using DRS

The second aim of this study was to analyze depth- and dose-dependent changes in vascular oxygenation after exposure to radiation. To determine depth-associated effects of radiation we conducted measurements using two different source-detectors separations SD = 1.5 mm and SD = 2.25 mm having different sampling depths of d = 0.8 mm and d = 1.8 mm, respectively. To determine dose-associated changes in oxygenation we performed single-dose radiotherapy with two different doses D = 2 Gy and D = 8 Gy.

Fig. 13 shows extracted total hemoglobin concentration and oxygen saturation for two different tumor volumes V = 100 mm^3 and V = 200 mm^3 and after exposure to radiation of D = 2 Gy and D = 8 Gy. We did not observe any volume-related changes in cHb or sO$_2$ (Fig. 13A-B, 13D-E). We also did not find any differences in sO$_2$ after exposure to radiation (Fig. 13E, 13F). However, we observed a significant change in cHb after exposure to 8 Gy of radiation for SD = 1.5 mm (p-value < 0.05) (Fig. 13C). Because radiation did not cause the change in sO$_2$, the decreased in cHb may be caused by disruptions in blood supply. We also observed significant differences in cHb measures between probes with SD = 1.5 mm and SD= 2.25 mm (p-value < 0.01 for V = 100 mm^3, p-value < 0.05 for V = 200 mm^3, p-value < 0.05 for before and after D = 2 Gy, p-value < 0.01 for before D = 8 Gy) (Fig. 13A, 13B, 13C). We associate these differences with physiologically different hemoglobin concentration at different tumor depths. We suggest this finding indicates a higher concentration of total hemoglobin and therefore higher blood supply in superficial layers of tumors.

Association between DRS-measured Vascular Oxygenation and Immunohistochemically Assessed Intracellular Hypoxia

The third aim of this study was to associate DRS-measured vascular oxygenation with an immunohistochemical assessment of intracellular hypoxia. Proposing the DRS method for radioresistance

identification, we hypothesized that DRS measures of vascular oxygenation can provide surrogate measures of cellular hypoxia. To test our hypothesis, we aimed to find the relationship between DRS-measured oxygenation in blood vessels and hypoxia within tumor cells. DRS optical measurements of cHb and sO_2 were described above. Fig. 14 shows mean values of immunohistochemically quantified hypoxic fraction for the same groups that were studied using DRS (at tumor volumes of V = 100 mm^3 and V = 200 mm^3, after radiotherapy of D = 2 Gy and D = 8 Gy) for two tumor depths 0.8 mm and 1.8 mm corresponding to the sampling depths of used source-detector separations SD = 1.5 mm and SD = 2.25 mm, respectively. From the obtained data, we did not observe any significant differences between groups which underwent single dose radiotherapy (Fig. 14). Interestingly, we observed a lower hypoxic fraction for the control group at the volume 200 mm^3 compared to radiation groups (Fig. 14A). However, it is important to note that it was impossible to conduct a reliable statistical analysis to compare between radiated and control groups due to small sample size of groups at V = 100 mm^3 and at V = 200 mm^3 (N<5). We suggest unexpected low values of hypoxic fraction for 200 mm^3o group may be a result of either poor perfusion of hypoxic drug.

In Fig. 15, we plotted measured pairs of hypoxic fraction and deoxygenated hemoglobin in order to determine the relationship between intracellular hypoxia and oxygenation within blood vessels. Although we did not observe significant correlation between deoxyhemoglobin and estimated hypoxia for groups irradiated with D = 2 Gy and D = 8 Gy we noticed that hypoxic fraction decreases with increased deoxyhemoglobin. We suggest that in the future experiments increasing sample sizes and adding extra data points may reveal correlation between hypoxia and concentration of deoxygenated hemoglobin.

IV.   Discussion

Diffuse reflectance spectroscopy is widely used for non-invasive measurements of tumor biology. While diffuse reflectance spectroscopy has been developing and finding more and more applications in biomedical research, multiple methods for extracting optical parameters from diffuse reflectance have been created. Some methods are based on photon transport simulations (e.g., Monte Carlo simulations, modified diffusion equation, P_3 approximation of transport equation, spatially resolved diffusion equation, spatially resolved Monte Carlo approximation, spatially resolved empirical method) whereas other models are solely based on experimental measurements of calibration phantoms (e.g., lookup table LUT inverse model) [28,31–35]. However, most of existing models rely on the assumption that tissue is a single layer of homogeneous turbid medium. It was stated before by multiples authors that this simplification of the tissue structure raises questions regarding the accuracy of extracted parameters [36,37]. Hennessy et. al. stated the importance of studying errors caused by one-layer assumptions. He has shown that for the Monte Carlo model oversimplification of tissue structure causes underestimation of hemoglobin and melanin concentrations as well as the correlation of these two parameters when SD = 250 μm is used. However, for the LUT-inverse model having wide applicability for various source-detector separations the effect of one-layer assumption has not been explored. In this study, fist time to our knowledge, we explored the impact of epidermal thickness on extracted optical properties using one-layer LUT model for fitting one- and two-layer spectra of real tissue (tumors with and without epidermis). Our major finding is that one-layer model applied to fit two-layer tissues may cause errors in the extraction of parameters for probes having source-detector separations close to the epidermal thickness. For SD = 350 μm we observed a significant positive correlation between scattering power and melanin concentration. Another important finding is that the one-layer LUT model fails to detect the absence of melanin when the epidermal layer is removed. We suggest that these findings indicate an LUT error in distinguishing scattering and absorbing contributions to the reflectance due to their similarity in the power-law spectral shape. In the future study, the model needs to be improved in order to eliminate the dependence between scattering power and melanin concentration and ensure correct estimation of scattering and absorption contributions. We also suggest that creating an LUT model that accounts for multilayered tissue would be

a significant advantage for applications using short source-detector separations. In the future work, to attest the obtained results, we are planning to analyze the effect of one-layer assumption on extracted parameters for two more source-detector separations: SD = 700 µm and SD = 1.5 mm.

Importantly, we did not observe the significant impact of the skin layer on DRS measurements of optical parameters using the probe with longer source-detector separation SD = 2.25 mm. In the next study, we chose the probe with SD = 2.25 mm along with SD = 1.5 mm to study dose- and depth-dependent changes in total hemoglobin concentration and oxygen saturation after exposure to ionizing radiation. As a result, we did not observe significant changes in cHb and sO_2 across groups having different tumors volumes. We also did not observe changes in the values of these parameters after exposure to 2 Gy or 8 Gy of radiation. However, multiple studies have demonstrated a radiation-induced increase in oxygenation in nude mice bearing head and neck xenografts using pO_2 microelectrodes and immunohistochemistry [38–40]. We suggest that the reason why we did not observe any changes in oxygenation is caused by the choice of the time point when we conducted DRS measurements. In our experiments, DRS was performed approximately one hour after the exposure to radiation. In the study done by Hu et. al., an increase in DRS-measured oxygenation was registered one day after exposure to radiation in head and neck xenografts [27]. Relying on the previously published information, we suggest that in future it will be important to study reoxygenation time points for tumor models used in our experiments. In vitro studies of cell oxygen consumption during radiation therapy could also provide us with important insights regarding changes happening within tumors during radiotherapy.

While we did not observe any dose-related effects on cHb and sO_2 after exposure to 2 Gy of radiation we found a significant change in cHb after exposure to D = 8 Gy. We suggest that this decrease may be caused by a disruption in blood supply caused by vasculature collapse. Our assumption is concordant with Park's work where he reported that exposure to a single-dose of radiation from 5 to 10 Gy causes mild vasculature damage in human tumor xenografts [41]. From the analysis of depth-dependent changes in cHb and sO_2, we found that measurements obtained with SD = 1.5 mm are significantly higher than cHb values measured by SD = 2 .25 mm. We associated these differences with physiological differences at different tumor depths (d = 0.8 mm and d = 1.8 mm, respectively) and concluded that this

finding may indicate a variability in blood supply within the tumor. Combing together significant change in cHb after exposure to 8 Gy of radiation at the depth of d = 0.8 mm and higher measures of cHb obtained by SD = 1.5 mm, we concluded that well developed vasculature on the surface of tumors gets damaged by high doses of radiation. We suggest that tumor is an inhomogeneous medium where blood vessels may not be evenly distributed resulting in hypoxia occurring in particular regions of a tumor. We believe that studying depth-dependent changes in tumor oxygenation is important for evaluating tumor response to radiation. Therefore, in the future, the goal of our laboratory will be to design multi-depth diffuse reflectance spectrometer (MDDRS) that would provide us with an important functional information about changes in tumor biology during radiotherapy.

In the second part of our study, we aimed to supplement DRS-obtained data with immunohistochemistry of hypoxia by pimonidazole. Our goal was to test the hypothesis that vascular sO_2 can be used as a marker of tumor intracellular hypoxia and to understand the relationship between DRS-measured vascular oxygenation and IHC-quantified hypoxia. As a result, we did not observe significant differences in IHC-quantified hypoxic fraction between control groups and groups irradiated with 2 Gy and 8 Gy of radiation. Maftei et al have found that the IHC-assessed hypoxia is decreased in FaDu xenografts one day after exposure to 10 Gy of radiation [39]. As was stated before for DRS measurements, we suggest that the reason why we did not observe radiation-induced effects in hypoxic fraction is caused by our choice of the measurement time point. In future, we are planning to investigate longitudinal changes in DRS-measured sO_2 and hypoxic fraction and the correlation between these two parameters at different time points after radiotherapy.

Interestingly, we observed lower values of the hypoxic fraction in the control group having tumor volume V = 200 mm[3] compared to other groups. However, due to the limited number of animals in control groups, we cannot conclude with confidence that this finding is physiologically relevant. In future, we are planning to increase the sample size to confirm the obtained result. Our assumption is that the unexpected decrease in the hypoxic fraction for this particular group may be caused by poor perfusion of the hypoxic drug. In the study done by Vishwanath et al, immunohistochemistry of pimonidazole was complemented with staining by perfusion marker Hoechst [8]. In future, we are planning to improve our

21

immunostaining protocol by staining of tumors for perfusion to ensure accurate quantification of intracellular hypoxia.

Due to the limited sample sizes, we also did not observe a significant correlation between quantified hypoxic fraction and concentration of deoxyhemoglobin within the blood. However, we noticed a nonsignificant negative correlation between hypoxic fraction and deoxyhemoglobin concentration for groups with N=7. Physiologically, it may be indicative of the correlation between cell oxygen demand and concentration of deoxyhemoglobin. Our assumption is that if tumor cells consume more oxygen more hemoglobin become deoxygenated. In future, more studies will be conducted to increase the sample size and to determine the relationship between intracellular hypoxia and vascular oxygenation during radiotherapy.

V. References

1. R. L. Siegel, K. D. Miller, and A. Jemal, "Cancer statistics, 2016," CA. Cancer J. Clin. **66**(1), 7–30 (2016) [doi:10.3322/caac.21332].

2. S. Marur and A. A. Forastiere, "Head and Neck Squamous Cell Carcinoma: Update on Epidemiology, Diagnosis, and Treatment," Mayo Clin. Proc. **91**(3), 386–396 (2016) [doi:10.1016/j.mayocp.2015.12.017].

3. "Head and Neck Cancers, Version 2.2013," <http://www.jnccn.org/content/11/8/917.short> (accessed 5 March 2017).

4. D. M. Brizel et al., "Tumor hypoxia adversely affects the prognosis of carcinoma of the head and neck," Int. J. Radiat. Oncol. Biol. Phys. **38**(2), 285–289 (1997).

5. M. F. Adam et al., "Tissue oxygen distribution in head and neck cancer patients," Head Neck **21**(2), 146–153 (1999).

6. A. Dietz et al., "Prognostic impact of reoxygenation in advanced cancer of the head and neck during the initial course of chemoradiation or radiotherapy alone," Head Neck **25**(1), 50–58 (2003) [doi:10.1002/hed.10177].

7. J. C. Walsh et al., "The Clinical Importance of Assessing Tumor Hypoxia: Relationship of Tumor Hypoxia to Prognosis and Therapeutic Opportunities," Antioxid. Redox Signal. **21**(10), 1516–1554 (2014) [doi:10.1089/ars.2013.5378].

8. K. Vishwanath et al., "Quantitative optical spectroscopy can identify long-term local tumor control in irradiated murine head and neck xenografts," J. Biomed. Opt. **14**(5), 054051-054051-4 (2009) [doi:10.1117/1.3251013].

9. K. Vishwanath et al., "Using Optical Spectroscopy to Longitudinally Monitor Physiological Changes within Solid Tumors," Neoplasia **11**(9), 889–900 (2009) [doi:10.1593/neo.09580].

10. "Head and Neck Cancer: Treatment Options," Cancer.Net, 25 June 2012, <http://www.cancer.net/cancer-types/head-and-neck-cancer/treatment-options> (accessed 5 March 2017).

11. R. Baskar et al., "Cancer and Radiation Therapy: Current Advances and Future Directions," Int. J. Med. Sci. **9**(3), 193–199 (2012) [doi:10.7150/ijms.3635].

12. J. A. Bertout, S. A. Patel, and M. C. Simon, "The impact of O2 availability on human cancer," Nat. Rev. Cancer **8**(12), 967–975 (2008) [doi:10.1038/nrc2540].

13. M. Höckel et al., "Intratumoral pO2 predicts survival in advanced cancer of the uterine cervix," Radiother. Oncol. J. Eur. Soc. Ther. Radiol. Oncol. **26**(1), 45–50 (1993).

14. M. Nordsmark, M. Overgaard, and J. Overgaard, "Pretreatment oxygenation predicts radiation response in advanced squamous cell carcinoma of the head and neck," Radiother. Oncol. J. Eur. Soc. Ther. Radiol. Oncol. **41**(1), 31–39 (1996).

15. P. L. Olive, "Radiation-induced reoxygenation in the SCCVII murine tumour: evidence for a decrease in oxygen consumption and an increase in tumour perfusion," Radiother. Oncol. **32**(1), 37–46 (1994) [doi:10.1016/0167-8140(94)90447-2].

16. L. Milas et al., "Role of Reoxygenation in Induction of Enhancement of Tumor Radioresponse by Paclitaxel," Cancer Res. **55**(16), 3564–3568 (1995).

17. C. Grau and J. Overgaard, "The Influence of Radiation Dose on the Magnitude and Kinetics of Reoxygenation in a C3H Mammary Carcinoma," Radiat. Res. **122**(3), 309–315 (1990) [doi:10.2307/3577761].

18. A. Ressel, C. Weiss, and T. Feyerabend, "Tumor oxygenation after radiotherapy, chemotherapy, and/or hyperthermia predicts tumor free survival," Int. J. Radiat. Oncol. **49**(4), 1119–1125 (2001) [doi:10.1016/S0360-3016(00)01523-6].

19. M. Nordsmark et al., "Prognostic value of tumor oxygenation in 397 head and neck tumors after primary radiation therapy. An international multi-center study," Radiother. Oncol. **77**(1), 18–24 (2005) [doi:10.1016/j.radonc.2005.06.038].

20. D. M. Brizel et al., "Oxygenation of head and neck cancer: changes during radiotherapy and impact on treatment outcome," Radiother. Oncol. **53**(2), 113–117 (1999) [doi:10.1016/S0167-8140(99)00102-4].

21. V. Rudat et al., "Predictive Value of the Tumor Oxygenation by Means of pO2 Histography in Patients with Advanced Head and Neck Cancer," Strahlenther. Onkol. **177**(9), 462–468 (2001) [doi:10.1007/PL00002427].

22. K. Newbold et al., "An Exploratory Study Into the Role of Dynamic Contrast-Enhanced Magnetic Resonance Imaging or Perfusion Computed Tomography for Detection of Intratumoral Hypoxia in Head-and-Neck Cancer," Int. J. Radiat. Oncol. **74**(1), 29–37 (2009) [doi:10.1016/j.ijrobp.2008.07.039].

23. P. J. Hoskin et al., "Hypoxia in Prostate Cancer: Correlation of BOLD-MRI With Pimonidazole Immunohistochemistry—Initial Observations," Int. J. Radiat. Oncol. **68**(4), 1065–1071 (2007) [doi:10.1016/j.ijrobp.2007.01.018].

24. A. R. Padhani et al., "Imaging oxygenation of human tumours," Eur. Radiol. **17**(4), 861–872 (2007) [doi:10.1007/s00330-006-0431-y].

25. P. J. Hoskin et al., "Dynamic contrast enhanced magnetic resonance scanning as a predictor of response to accelerated radiotherapy for advanced head and neck cancer.," Br. J. Radiol. **72**(863), 1093–1098 (1999) [doi:10.1259/bjr.72.863.10700827].

26. T. Lister, P. A. Wright, and P. H. Chappell, "Optical properties of human skin," J. Biomed. Opt. **17**(9), 0909011–09090115 (2012) [doi:10.1117/1.JBO.17.9.090901].

27. F. Hu et al., "Oxygen and Perfusion Kinetics in Response to Fractionated Radiation Therapy in FaDu Head and Neck Cancer Xenografts Are Related to Treatment Outcome," Int. J. Radiat. Oncol. **96**(2), 462–469 (2016) [doi:10.1016/j.ijrobp.2016.06.007].

28. G. M. Palmer and N. Ramanujam, "Monte Carlo-based inverse model for calculating tissue optical properties. Part I: Theory and validation on synthetic phantoms," Appl. Opt. **45**(5), 1062–1071 (2006) [doi:10.1364/AO.45.001062].

29. N. Rajaram, T. H. Nguyen, and J. W. Tunnell, "Lookup table–based inverse model for determining optical properties of turbid media," J. Biomed. Opt. **13**(5), 050501-050501-3 (2008) [doi:10.1117/1.2981797].

30. C. P. Sabino et al., "The optical properties of mouse skin in the visible and near infrared spectral regions," J. Photochem. Photobiol. B **160**, 72–78 (2016) [doi:10.1016/j.jphotobiol.2016.03.047].

31. G. Zonios et al., "Diffuse reflectance spectroscopy of human adenomatous colon polyps in vivo," Appl. Opt. **38**(31), 6628–6637 (1999) [doi:10.1364/AO.38.006628].

32. J. C. Finlay and T. H. Foster, "Hemoglobin oxygen saturations in phantoms and in vivo from measurements of steady- state diffuse reflectance at a single, short source- detector separation," Med. Phys. **31**(7), 1949–1959 (2004) [doi:10.1118/1.1760188].

33. N. Ghosh et al., "Measurement of optical transport properties of normal and malignant human breast tissue," Appl. Opt. **40**(1), 176–184 (2001) [doi:10.1364/AO.40.000176].

34. P. Thueler et al., "In vivo endoscopic tissue diagnostics based on spectroscopic absorption, scattering, and phase function properties," J. Biomed. Opt. **8**(3), 495–503 (2003) [doi:10.1117/1.1578494].

35. T. J. Pfefer et al., "Reflectance-based determination of optical properties in highly attenuating tissue," J. Biomed. Opt. **8**(2), 206–215 (2003) [doi:10.1117/1.1559487].

36. R. Hennessy, M. K. Markey, and J. W. Tunnell, "Impact of one-layer assumption on diffuse reflectance spectroscopy of skin," J. Biomed. Opt. **20**(2), 027001–027001 (2015) [doi:10.1117/1.JBO.20.2.027001].

37. G. Zonios and A. Dimou, "Modeling diffuse reflectance from semi-infinite turbid media: application to the study of skin optical properties," Opt. Express **14**(19), 8661–8674 (2006) [doi:10.1364/OE.14.008661].

38. W. Harriss et al., "Measurement of reoxygenation during fractionated radiotherapy in head and neck squamous cell carcinoma xenografts," Australas. Phys. Eng. Sci. Med. **33**(3), 251–263 (2010) [doi:10.1007/s13246-010-0032-6].

39. C.-A. Maftei et al., "Changes in the fraction of total hypoxia and hypoxia subtypes in human squamous cell carcinomas upon fractionated irradiation: Evaluation using pattern recognition in microcirculatory supply units," Radiother. Oncol. **101**(1), 209–216 (2011) [doi:10.1016/j.radonc.2011.05.023].

40. A. Ressel, C. Weiss, and T. Feyerabend, "Tumor oxygenation after radiotherapy, chemotherapy, and/or hyperthermia predicts tumor free survival," Int. J. Radiat. Oncol. **49**(4), 1119–1125 (2001) [doi:10.1016/S0360-3016(00)01523-6].

41. H. J. Park et al., "Radiation-Induced Vascular Damage in Tumors: Implications of Vascular Damage in Ablative Hypofractionated Radiotherapy (SBRT and SRS)," Radiat. Res. **177**(3), 311–327 (2012) [doi:10.1667/RR2773.1].
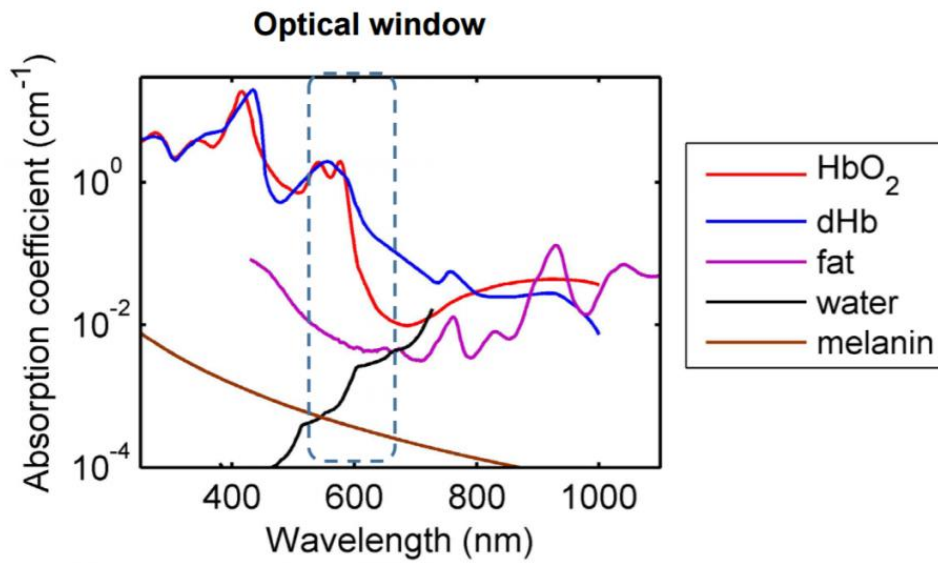
Figure 1. Absorption spectra of tissue components mainly contributing to the absorption of light in the range of 300-100 nm: oxygenated hemoglobin HbO_2, deoxygenated hemoglobin dHb, fat, water, and melanin.
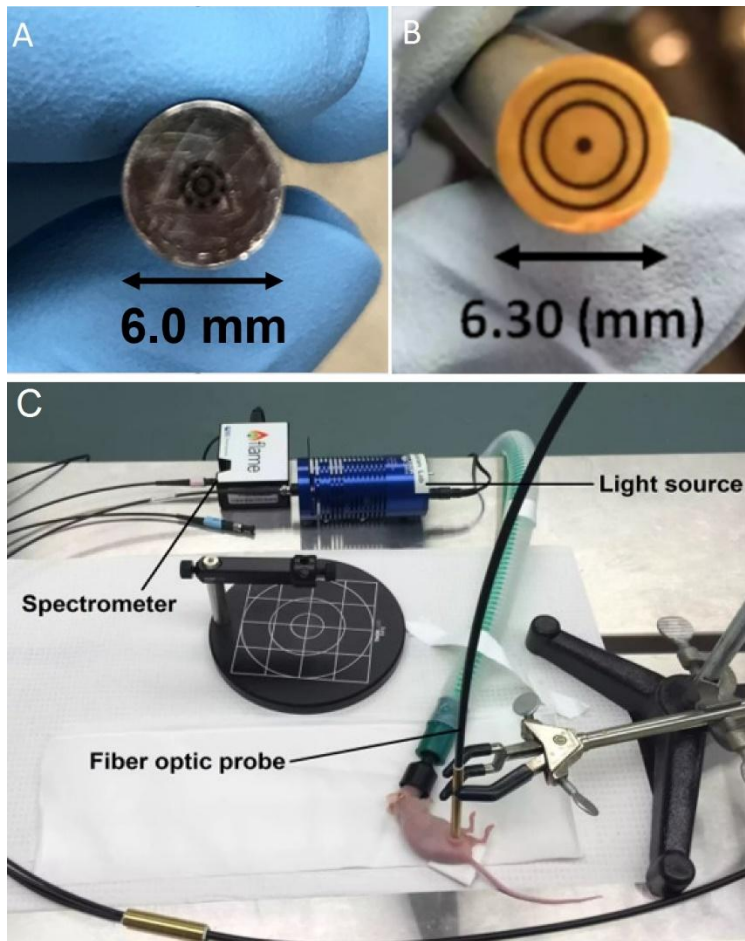
Figure 2. Diffuse Reflectance Spectroscopy (DRS) system. (A) Optical fiber probe with source-detector separations SD = 350 µm and SD = 700 µm. (B) Optical fiber probe with source-detector separations SD = 1.5 mm and SD = 2.25 mm. (C) Diffuse Reflectance Spectroscopy (DRS) system containing light source, spectrometer, and optical fiber prove.

Figure 3. Radiotherapy performed in biological X-ray radiator (X-RAD 320, Precision X-ray).
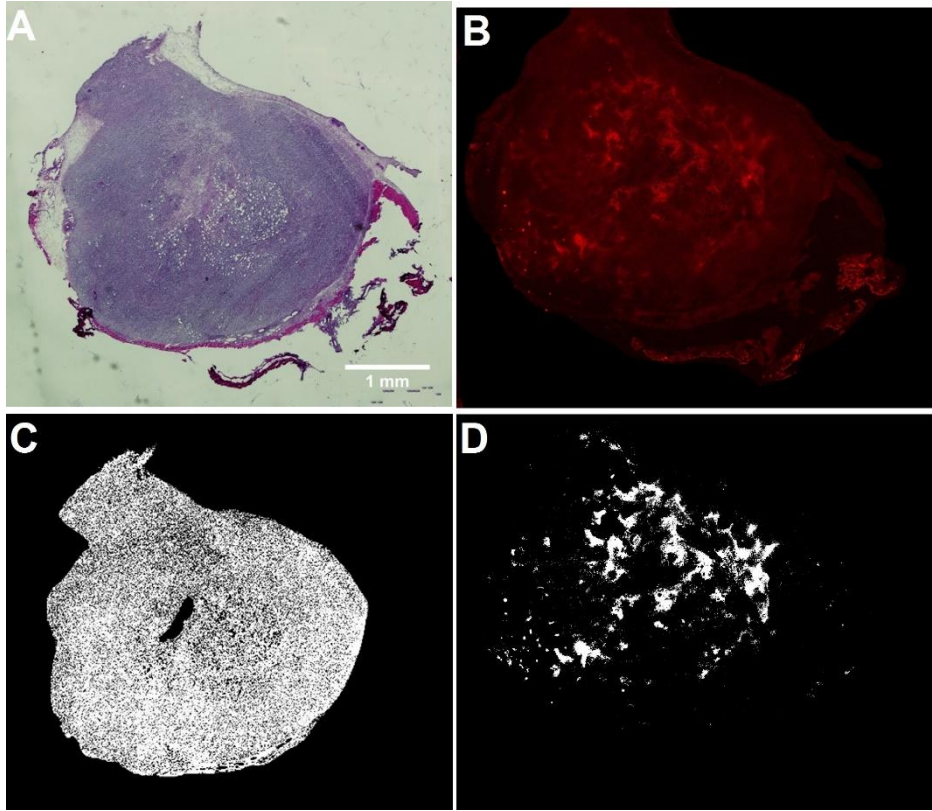
Figure 4. Representative images of H&E staining and pimonidazole immunostaining of a tumor. (A) Representative image of H&E staining. (B) Representative image of immunostaining by pimonidazole. (C) Black and white mask of H&E staining for quantification of total tumor area and tumor necrotic area. (D) Black and white mask of pimo-stained section for quantification of tumor hypoxic fraction.
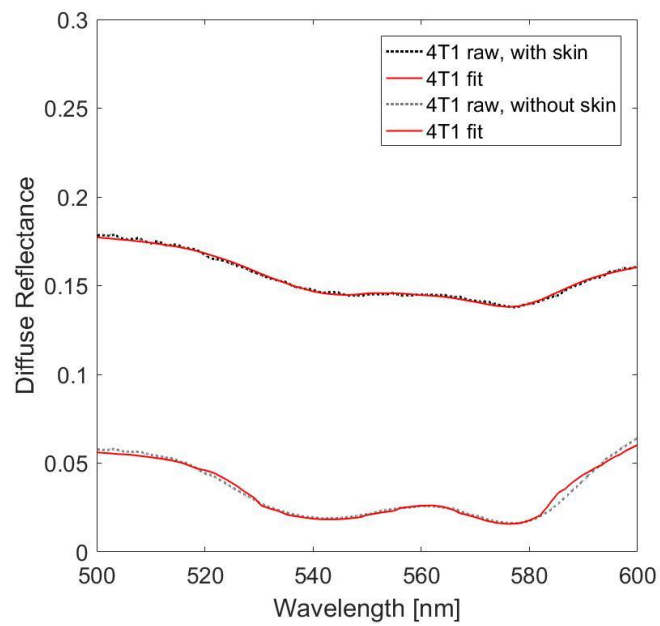
Figure 5. Representative diffuse reflectance spectra obtained for 4T1 tumor using SD = 350 μm before and after skin was removed.
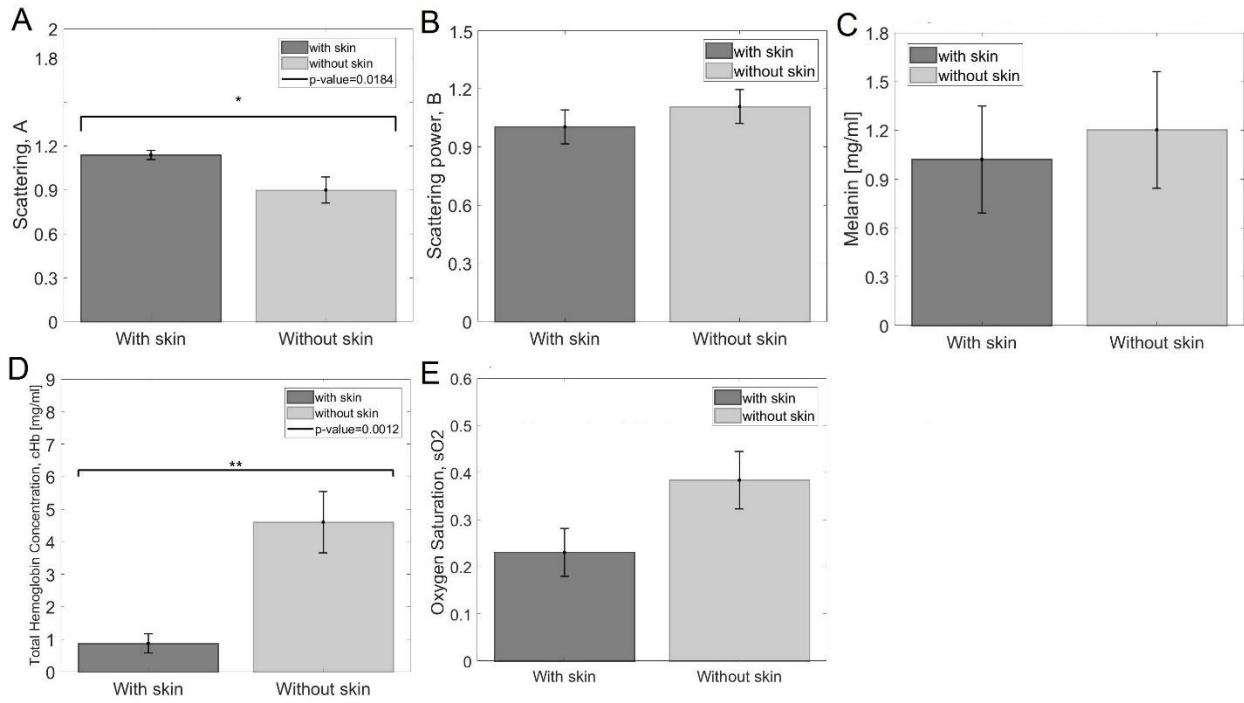
Figure 6. Extracted parameters before and after skin was removed (SD = 350 µm). Error bars represent standard errors. (A) Scattering, A. (B) Scattering power, B. (C) Melanin concentration. (D) Total hemoglobin concentration, cHb. (E) Oxygen saturation, sO_2.
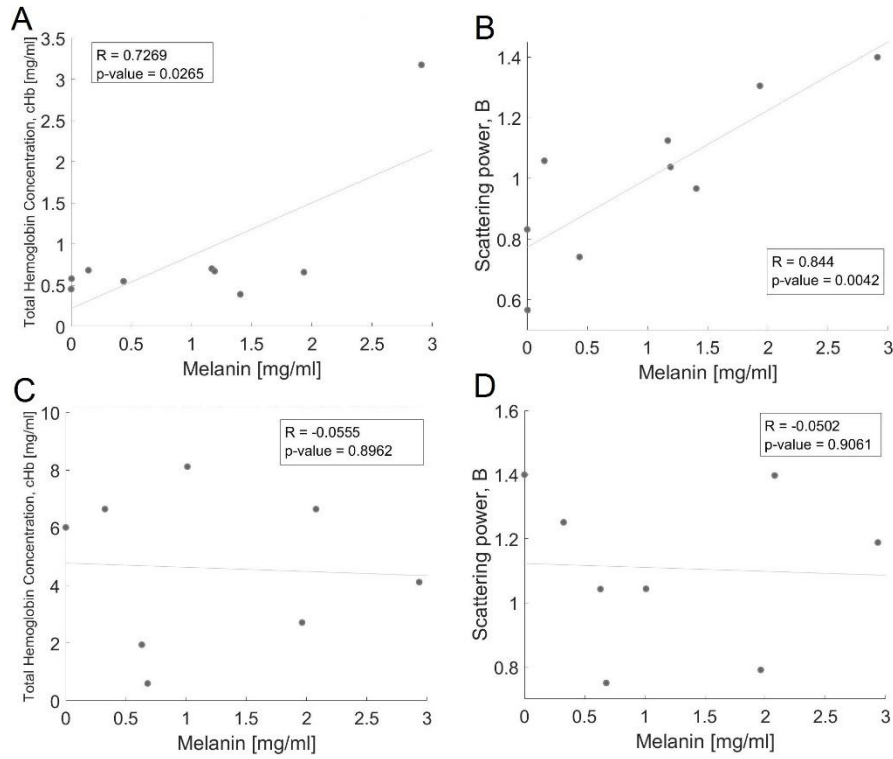
Figure 7. Scatter plots of measured pairs of total hemoglobin concentration cHb, melanin concentration, and scattering power B for SD = 350 µm. (A) Correlation between cHb and melanin when one-layer model is applied to two-layer spectra. (B) Correlation between B and melanin when one-layer model is applied to two-layer spectra. (C) Correlation between cHb and melanin when one-layer model is applied to one-layer spectra. (D) Correlation between B and melanin when one-layer model is applied to one-layer spectra.
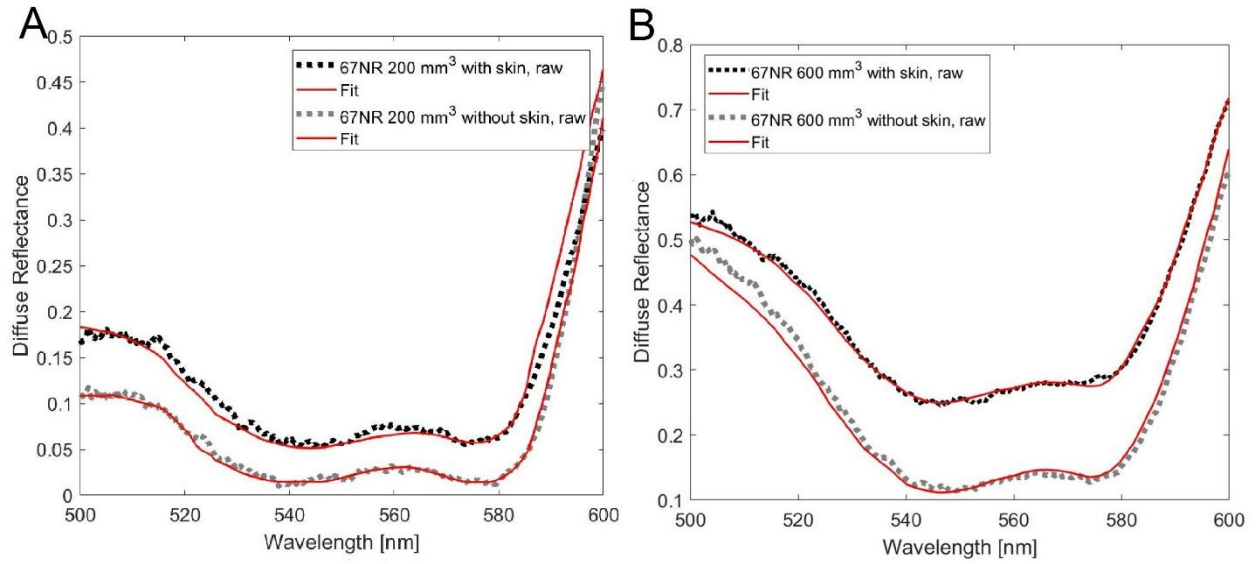
Figure 8. Representative diffuse reflectance spectra obtained for 67NR tumor at the volume V = 200 mm^3 (A) and for 67NR tumor at the volume V = 600 mm^3 (B) before and after skin was removed (SD = 2.25 mm).
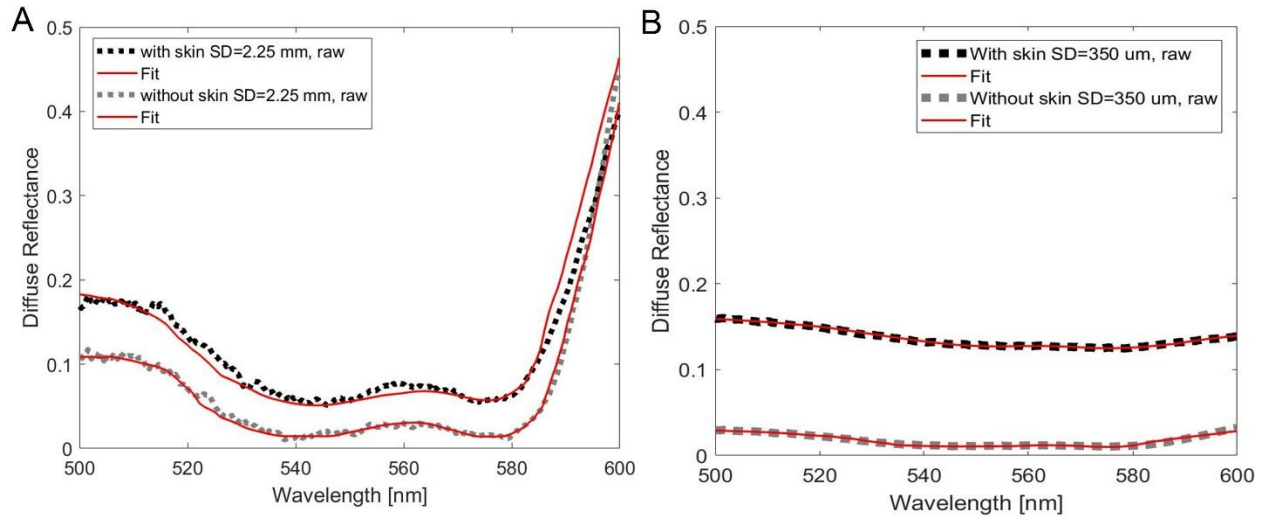
Figure 9. Representative diffuse reflectance spectra obtained for two 67NR tumors at the equal volume V = 200 mm^3 when SD = 2.25 mm is used (A) and when SD = 350 μm is used (B).
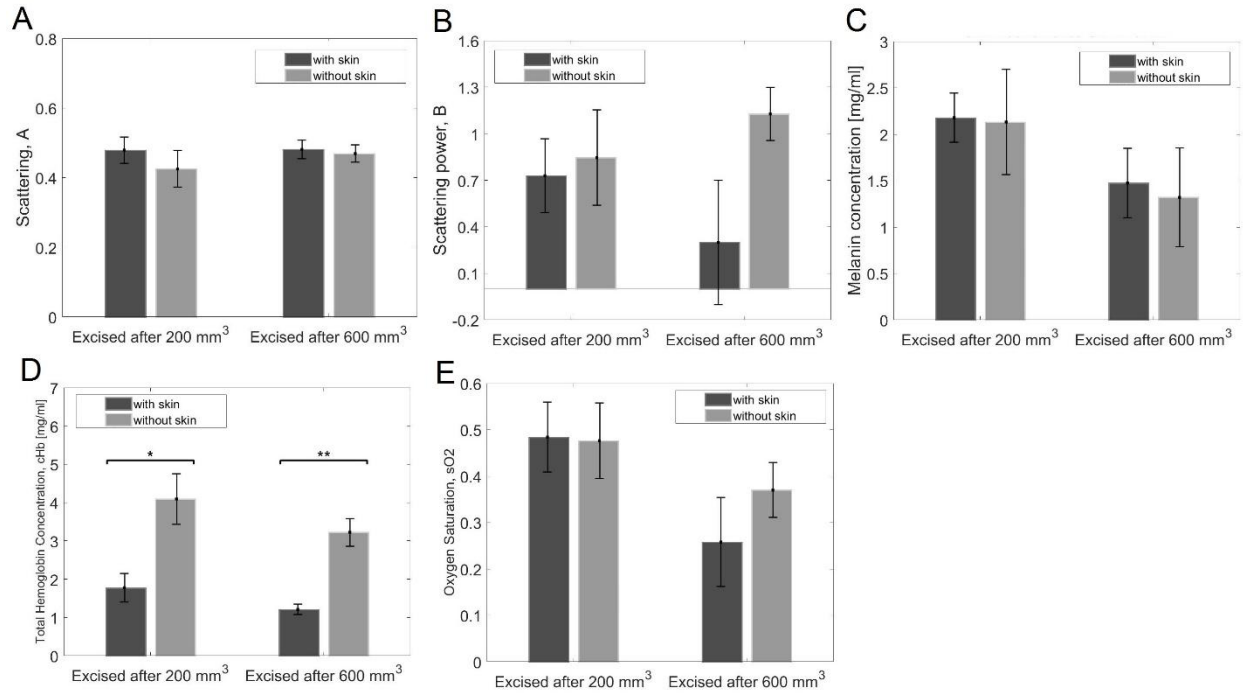
Figure 10. Extracted parameters before and after skin was removed for experimental groups excised at tumor volumes V = 200 mm^3 and V = 600 mm^3 (SD = 2.25 mm). Error bars represent standard errors. (A) Scattering, A. (B) Scattering power, B. (C) Melanin concentration. (D) Total hemoglobin concentration, cHb. (E) Oxygen saturation, sO$_2$.
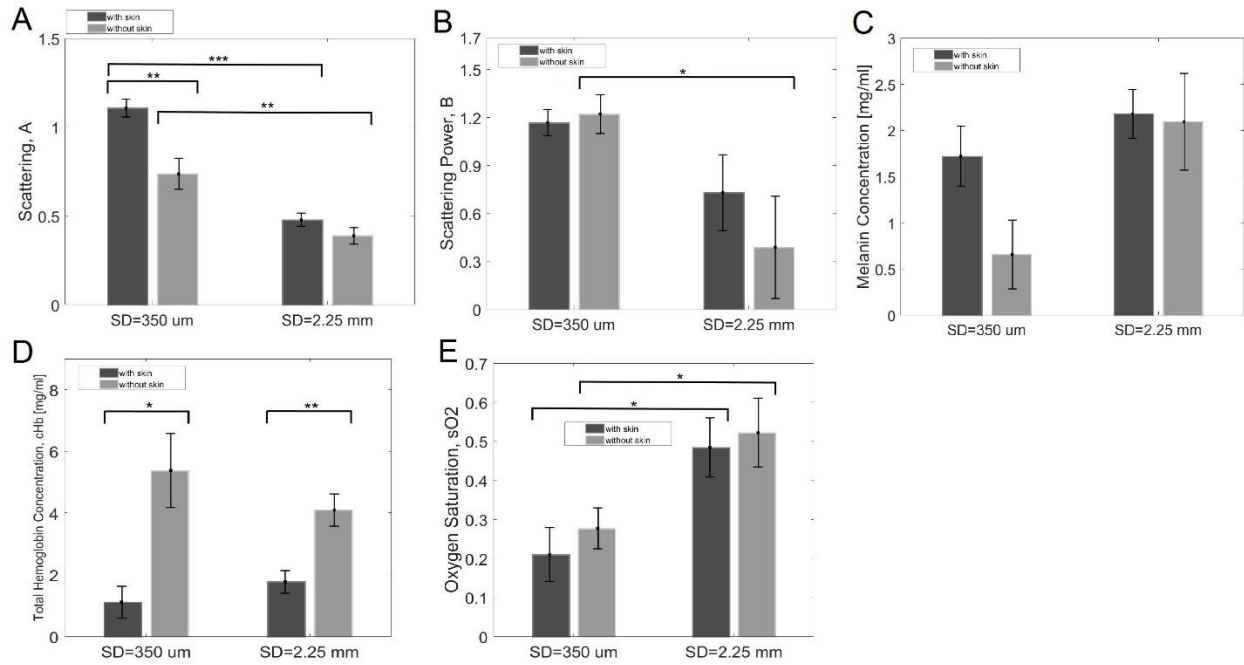
Figure 11. Parameters extracted from DRS-measured spectra of 67NR tumors at the volume V=200 mm^3 using SD = 350 μm and SD = 2.25 mm. Error bars represent standard errors. (A) Scattering, A. (B) Scattering power, B. (C) Melanin concentration. (D) Total hemoglobin concentration, cHb. (E) Oxygen saturation, sO$_2$.
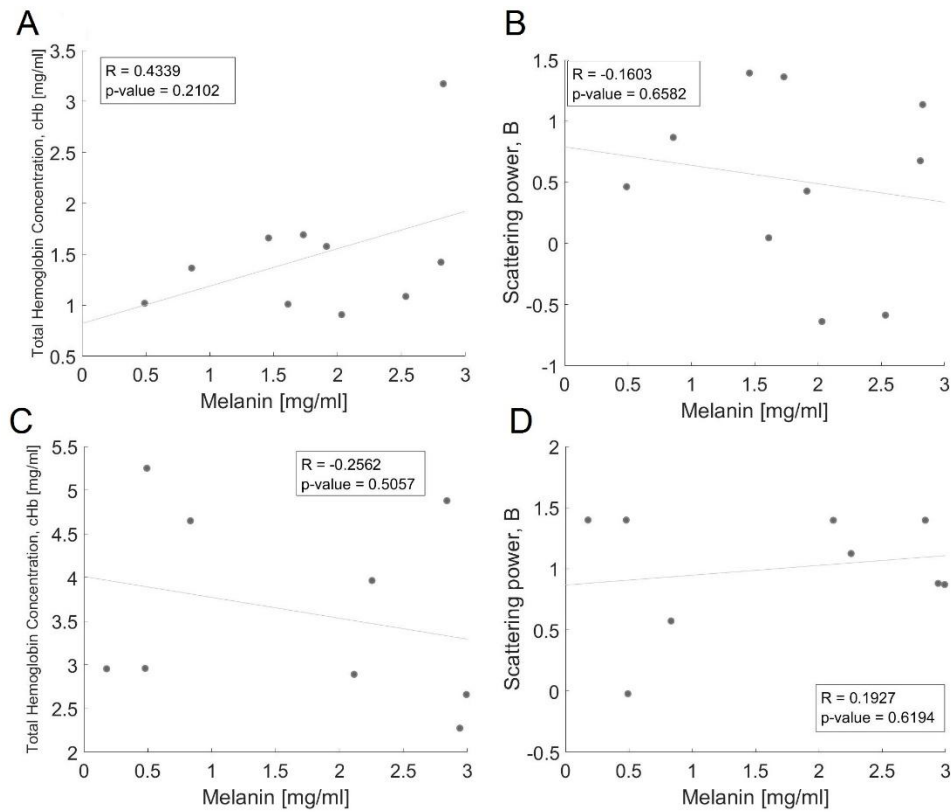
Figure 12. Scatter plots of measured pairs of total hemoglobin concentration cHb, melanin concentration, and scattering power B for SD = 2.25 mm. (A) Correlation between cHb and melanin when one-layer model is applied to two-layer spectra. (B) Correlation between B and melanin when one-layer model is applied to two-layer spectra. (C) Correlation between cHb and melanin when one-layer model is applied to one-layer spectra. (D) Correlation between B and melanin when one-layer model is applied to one-layer spectra.
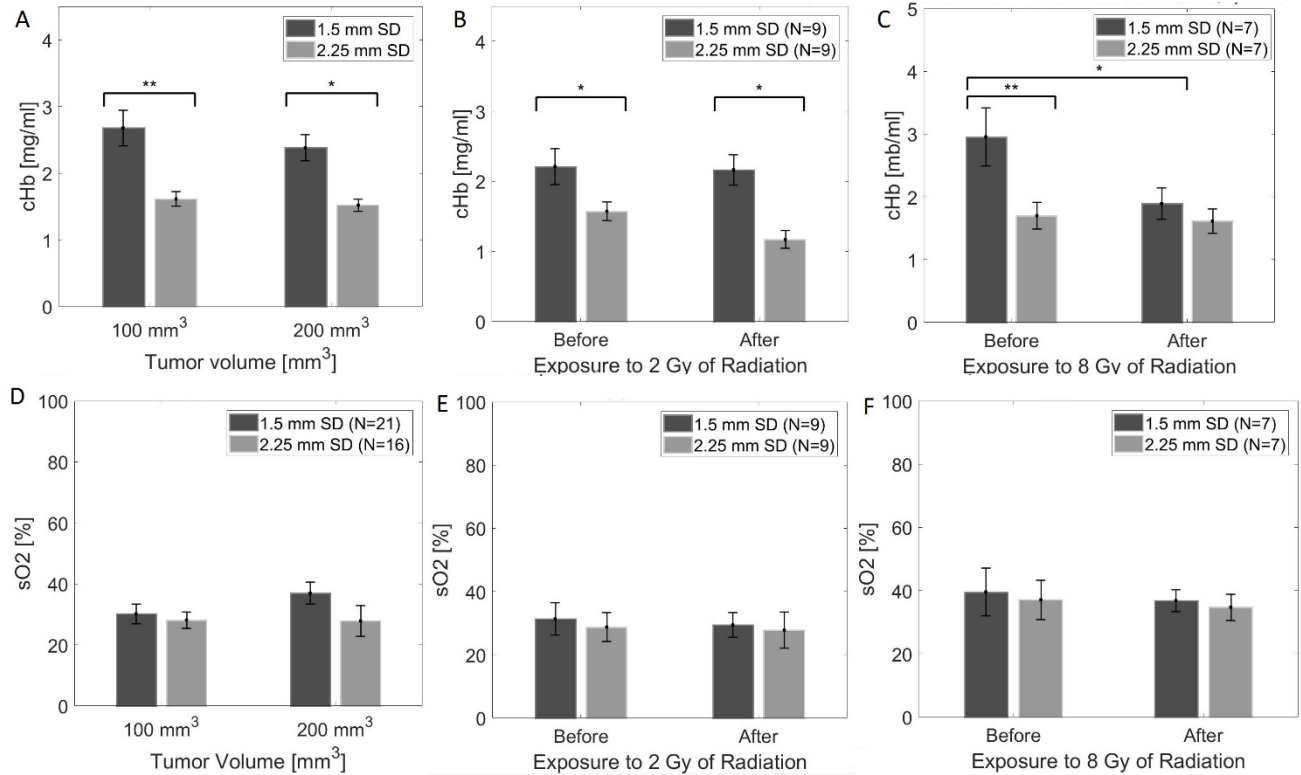
Figure 13. Extracted concentration of total hemoglobin cHb and oxygen saturation sO_2 from tumors at volumes $V = 100$ mm^3 and $V = 200$ mm^3 and after exposure to 2 and 8 Gy of radiation using two source-detector separations SD = 1.5 mm and SD = 2.25 mm. Error bars represent standard errors. (A) Hemoglobin concentration of tumors at $V = 100$ mm^3 and $V = 200$ mm^3. (B) Hemoglobin concentration before and after exposure to 2 Gy of radiation. (C) Hemoglobin concentration before and after exposure to 8 Gy of radiation. (D) Tumor oxygen saturation at $V = 100$ mm^3 and $V = 200$ mm^3. (E) Tumor oxygen saturation before and after exposure to 2 Gy of radiation. (F) Tumor oxygen saturation before and after exposure to 8 Gy of radiation.
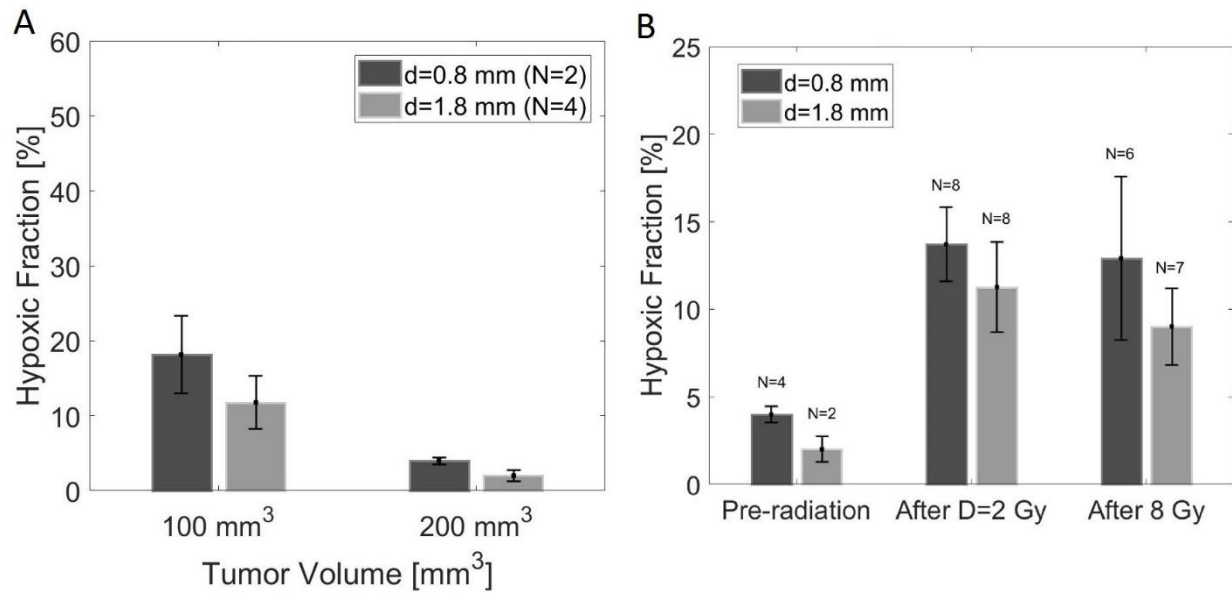
Figure 14. Hypoxic fraction quantified from immunohistochemistry of intracellular hypoxia for two tumor depths d = 0.8 mm and d = 1.8 mm at volumes V = 100 mm^3 and V = 200 mm^3 and after exposure to 2 and 8 Gy of radiation. Error bars represent standard errors. (A) Hypoxic fraction quantified at tumor volumes V = 100 mm^3 and V = 200 mm^3. (B) Hypoxic fraction quantified after exposure to 2 and 8 Gy of radiation.
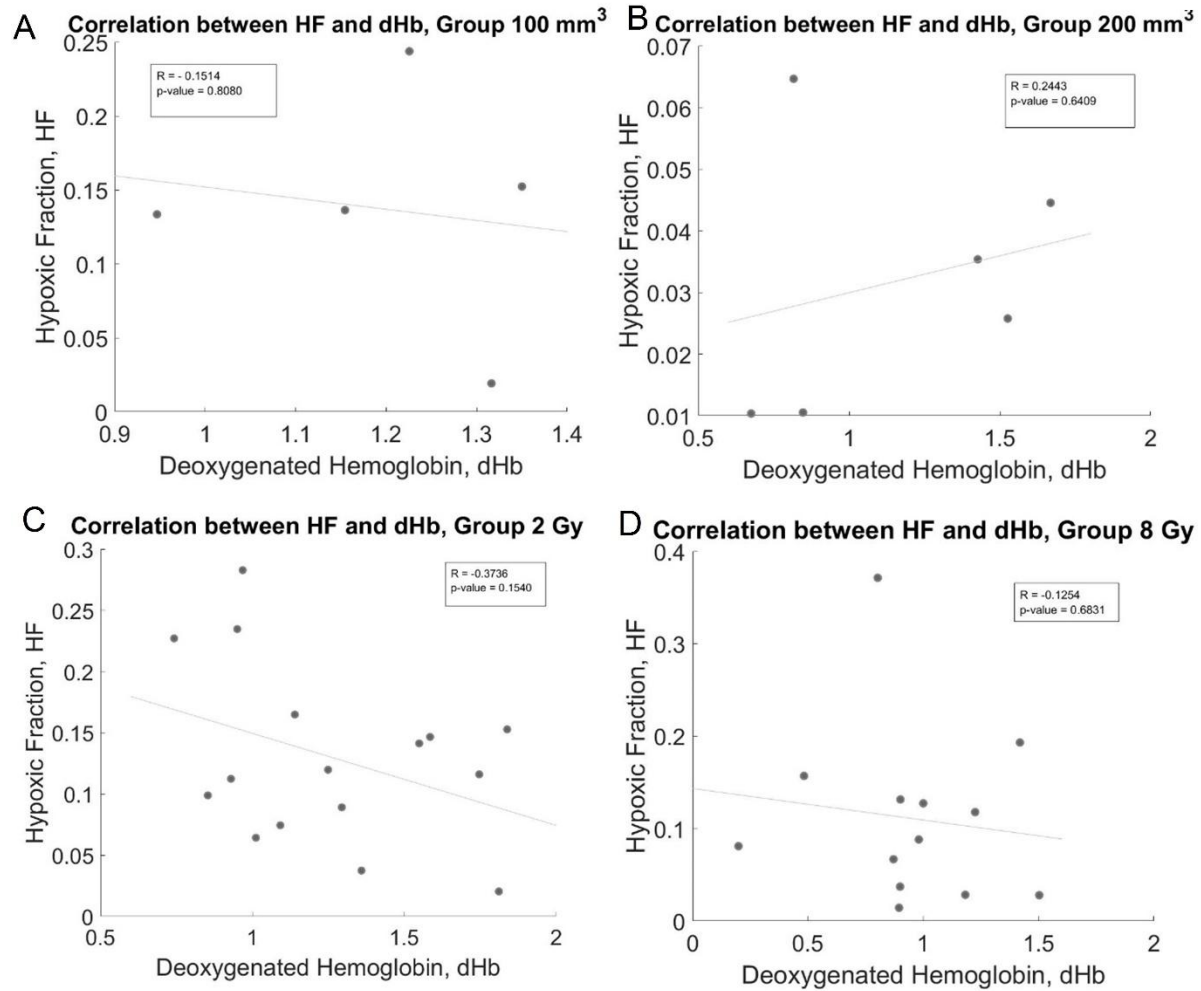
Figure 15. Scatter plots of measured pairs of hypoxic fraction H and deoxygenated hemoglobin dHb for all experimental groups. (A) Correlation between HF and dHb for tumors at the volume V = 100 mm^3. (B) Correlation between HF and dHb for tumors at the volume V = 200 mm^3. (C) Correlation between HF and dHb for tumors which underwent exposure to 2 Gy radiation. (D) Correlation between HF and dHb for tumors which underwent exposure to 8 Gy radiation.

VII. Appendix A: IACUC Protocol Approval #15035

UNIVERSITY OF ARKANSAS

Office of Research Compliance

MEMORANDUM

TO: Narashimhan Rajaram

FROM: Craig N. Coon, Chairman

DATE: Feb 6, 2015

SUBJECT: IACUC Approval

Expiration Date: Feb 7, 2018

The Institutional Animal Care and Use Committee (IACUC) has APPROVED your
Protocol: 15035 Intravital microscopy of tumor oxygenation and
metabolismin metastatic and non-metastatic breast cancers to begin Feb 8, 2015

In granting its approval, the IACUC has approved only the information provided. Should
there be any further changes to the protocol during the research, please notify the IACUC
in writing (via the Modification form) prior to initiating the changes. If the study period is
expected to extend beyond Feb 7, 2018 you must submit a newly drafted protocol
prior to that date to avoid any interruption. By policy the IACUC cannot approve a study for
more than 3 years at a time.

The IACUC appreciates your cooperation in complying with University and Federal
guidelines involving animal subjects.

CNC/aem

cc: Animal Welfare Veterinarian

VIII. Appendix B: IACUC Protocol Approval #15035

UNIVERSITY OF
ARKANSAS.

Office of Research Compliance

MEMORANDUM

To: Narasimhan Rajaram

From: Craig Coon, IACUC Chair

Date: June 03, 2016

Subject: IACUC Approval

Expiration Date: February 7, 2018

The Institutional Animal Care and Use Committee (IACUC) has APPROVED your personnel additions of Daria Semeniak and Raisa Rasul to protocol # 15035 "Intravital microscopy of tumor oxygenation and metabolism in metastatic and non-metastatic breast cancers".

In granting its approval, the IACUC has approved only the information provided. Should there be any further changes to the protocol during the research, please notify the IACUC in writing (via the Modification form) prior to initiating the changes. If the study period is expected to extend beyond February 7, 2018 you must submit a newly drafted protocol prior to that date to avoid any interruption. By policy the IACUC cannot approve a study for more than 3 years at a time.

The IACUC appreciates your cooperation in complying with University and Federal guidelines involving animal subjects.

CNC/aem
cc: Animal Welfare Veterinarian